ACADEMIA QUANTUM

Research article
Published: 2024-10-23
https://doi.org/10.20935/AcadQuant7374

# Pulse family optimization for parameterized quantum gates using spectral clustering

Robert de Keijzer[1,2,*], Jurgen Snijders[2,3], André Carvalho[3], Servaas Kokkelmans[1,2]

Academic Editors: Randy Kuang, Yuhua Duan

## Abstract

Parameterized gate circuits are used in many applications in the current Noisy Intermediate-Scale Quantum (NISQ) era of quantum computing. These parameterized gates are mainly implemented using analytically found pulse protocols, often yielding suboptimal gate times, and consequently, fidelities. Alternatively, gate optimization algorithms are designed to construct high-fidelity pulses for individual fixed points in a continuous parameter space. Gates for intermediate parameters can subsequently be found by some form of interpolation between previously constructed pulses. Nevertheless, it is not guaranteed (as with analytic protocols) that the pulses found by the optimization algorithms belong to the same *family* of solutions and thus resemble each other. Interpolation of two pulses from different solution families often leads to high infidelities, as the pulse strays away from the minimum in the parameter/fidelity landscape. This work introduces a *spectral clustering* method to sort high-fidelity, optimized pulses in families and interpolate solely between pulses of the same family. Accordingly, interpolations will always approach maximal fidelity. Furthermore, as more than one pulse family is constructed, the parameter space can be partitioned, and according to this partition, a family prevails fidelity-wise. This work provides a meticulous demonstration of our constitutive continuous gate family construction by applying it to a universal gate set for Rydberg and Cat qubits under noise.

**Keywords:** *quantum computing, Rydberg, pulse construction, pulse families, continuous gate sets*

**Citation:** de Keijzer R, Snijders J, Carvalho A, Kokkelmans S. Pulse family optimization for parameterized quantum gates using spectral clustering. *Academia Quantum* 2024;1. https://doi.org/10.20935/AcadQuant7374

## 1. Introduction

In order for a quantum computer to be able to perform all possible computations, it has to possess the ability to execute a universal gate set, consisting of all possible single-qubit rotations and at least one entangling two-qubit operation [1]. The canonical single-qubit gate set consists of the rotation gates over angle $\theta$: $R_X(\theta), R_Y(\theta),$ and $R_Z(\theta)$, which form the basis for many variational quantum algorithms (VQAs) [2]. These parameterized gates are executed in physical systems using some control function on the qubits, i.e., laser pulses or electrical currents, specific to each individual parameter. Currently, quantum computing systems are in the Noisy Intermediate-Scale Quantum (NISQ) era, where qubits are highly susceptible to noise [3]. This means that it is important to choose the optimal control function to mitigate noise, which is often not a standard analytical protocol, but some faster control pulse as constructed by a pulse optimization algorithm [4–9]. These variational methods often lead to faster pulses with higher fidelity as a result.

The problem with these optimization algorithms is that, unlike analytical protocols, they only prescribe pulses for one fixed point in the parameter space at a time, and not for the entire continuous set of parameters, which is especially relevant for VQAs [10–12], where many different parameter realizations are necessary. For constructing control pulses, a new unique parameter is required every time, which is too expensive computationally, making it infeasible in majority of VQAs. The task at hand is to extend a collection of solutions for discrete points in a parameter space to the entire continuous set by some form of interpolation. However, this approach has an underlying complication. Assume a set of $M$ subsequent and close points in the gate parameter space $\{\theta_i\}_i^M$, for which one wishes to optimize the pulses. Initially, the pulse optimization algorithm will find a local minimizing pulse for $\theta_0$, and as the optimization problem is regular, there will be a corresponding local minimizing pulse for $\theta_1$ as long as the two values for $\theta$ are close enough. In general, there exist corresponding pulse solutions for each $\theta_i$, which we then call a pulse *family*, as introduced in [13]. Interpolating within a pulse family will yield pulses for intermediate values of $\theta$, with comparatively high fidelities. The problem, however, is that there is no guarantee that for every value of $\theta_i$, matching local minima will be found, and thus there is no guarantee that all the found optimized pulses will belong to a single family. Interpolating *between* two pulse families will generally yield lower fidelities because the resulting pulses will not be in local minima of the pulse/fidelity landscape (see **Figure 1**).

Previous work has been done on the construction of high-fidelity continuous gate sets. In [4, 9, 14], pulses that mitigate hardware

[1]Department of Applied Physics, Eindhoven University of Technology, 5600 MB Eindhoven, Noord-Brabant, The Netherlands.
[2]Eindhoven Hendrik Casimir Institute, Eindhoven University of Technology, 5600 MB Eindhoven, Noord-Brabant, The Netherlands.
[3]Q-CTRL, Chippendale, NSW 2008, Australia.
[*]email: r.j.p.t.d.keijzer@tue.nl

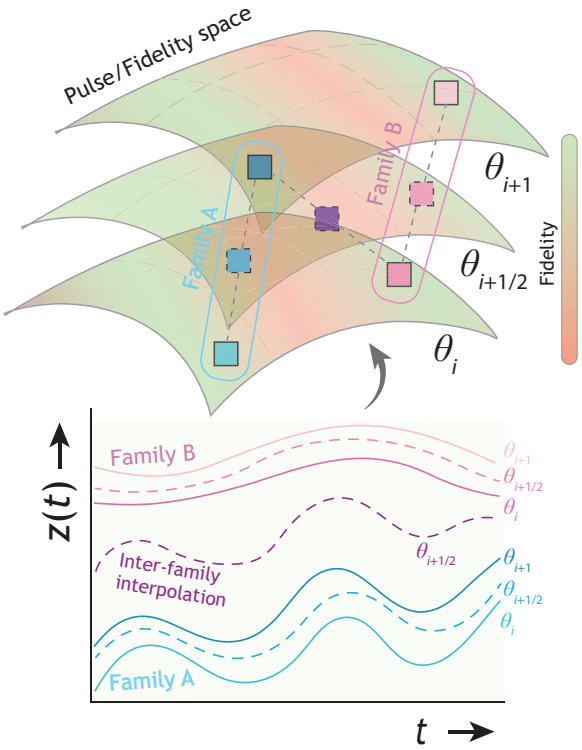


**Figure 1** • Graphical representation of the pulse interpolation problem. A pulse optimization algorithm might find one of the several local minimizing pulses for $\theta_i$ and $\theta_{i+1}$. If these are corresponding local minima, the pulses belong to the same family (blue or pink) and interpolation yields a pulse for $\theta_{i+1/2}$ with a high fidelity. If the minima do not correspond, interpolation happens between pulses of different families, yielding a pulse for $\theta_{i+1/2}$ with a low fidelity (purple).

errors were constructed based on a parameterized Hamiltonian. These results are extended to the continuous case in [15]. The study in [16] is the first to mention the problem of similarity between pulses, but the study was only related to single-parameter optimization. In [13, 17–19], methods that optimize continuous gate sets were devised while maintaining pulse similarity across different parameters for interpolation purposes. In [13, 17], a neural network approach was used, where the networks were trained by randomly sampling the parameter space. The disadvantage of such a black-box method is that verification of the resulting pulses is nontrivial. In [18], Trotterization was used to implement continuous parameter exponential matrices, but the study did not account for time optimization. The work in [19] utilizes the Tikhonov regularization and feedforward to enforce pulse similarity, and this is partly employed in our method. However, our work is the first to utilize clustering methods from the graph theory [20, 21] to find multiple families of gates, which has three main advantages over all previous methods:

- First, partitioning the parameter space according to where certain pulse families outperform the others has the potential to yield exceedingly higher fidelities than a singular family approach.
- Finding multiple families allows for the selection of pulses that are best suited to experimental procedures after verification on a setup.
- The clustering method provides a more well-suited manner of interpolating pulses using Wasserstein-2 distances from optimal transport (see Section 3).

The layout of this article is as follows. Section 2.1 describes optimal control methods used to construct optimal pulses for discrete parameter values $\theta_i$. Section 2.2 prescribes our pulse family clustering algorithm, its relation to other methods, and its advantages. Section 2.3 details the interpolation methods employed in this work. In Section 3, we show initial results for our approach, starting with results on the Wasserstein-2 distance to characterize pulse similarity in Section 3.1 Section 3.2 illustrates the increases in fidelities our method has for interpolation. Finally, Section 4 summarizes and presents a future outlook.

## 2. Materials and methods

### 2.1. Pulse optimization

The application analyzed in this work is creating a universal parameterized gate set of $R_X(\theta), R_Y(\theta), R_Z(\theta)$, and $R_{ZZ}(\theta)$, where $\theta \in [0, \pi]$. This will be performed on the Rydberg qubits [22, 23], an architecture that recently has become exceedingly mature, and also on Cat qubits [24, 25], which recently are gaining traction within the quantum computing community. This illustrates the versatility of our methods. In this section, we briefly describe the optimization procedure for fixed parameters $\theta_i$, which has been well described in literature [2, 26, 27]. The evolution of the qubit system density matrix $\rho_t$ follows a Lindblad equation [28] of the form

$$\begin{aligned} \partial_t \rho_t &= -i\big[H_{\text{sys}}[z(t)], \rho_t\big] + \mathcal{L}(\rho_t), \quad \rho(0) = \rho_0, \\ \mathcal{L}(\rho) &= \sum_k \gamma_k V_k \rho V_k - \frac{1}{2}\gamma_k \{V_k^\dagger V_k, \rho\}, \end{aligned} \tag{1}$$

where $H_{\text{sys}}[z(t)]$ is the system's Hamiltonian controlled by user-defined and optimizable pulses $z(t)$ and $\mathcal{L}$ is the Lindblad operator responsible for the different sources of decoherence in the system. $V_k$ and $\gamma_k$ are the jump operators with corresponding strengths, defining the Lindblad operator. The pulses are functions on $[0, T]$, where $T$ is the gate end time, bounded by experimental limitations as $z_{\min} \leq z(t) \leq z_{\max}$. The physical interpretation of the pulse type is system specific. In Rydberg systems, we can control the transitions between the $|0\rangle$, $|1\rangle$, and $|r\rangle$ states on qubit $j$ using coupling strengths $\Omega_{ab,j}$ and detunings $\Delta_{b,j}$ on transition $|a\rangle \leftrightarrow |b\rangle$ to get $z(t) \in \{\Omega_{01,j}(t), \Delta_{1,j}(t), \Omega_{1r,j}(t), \Delta_{r,j}\}$ [2]. Meanwhile, Cat qubits offer control on the single-photon drive $E_j(t)$, the detuning $\Delta_j(t)$, the interaction strength $g(t)$, and the two-photon drive $G_j(t)$ [24]. This gives $z(t) \in \{E_j(t), \Delta_j(t), G_j(t), g(t)\}$. For the Rydberg and Cat qubit systems, we introduce characteristic timescales $\tau_{\text{Ryd}} = 1/\Omega_{\max}$ and $\tau_{\text{Cat}} = 1/K$, respectively, where $\Omega_{\max}$ is a maximal coupling strength in the Rydberg system and $K$ is the Kerr nonlinearity in the Cat qubit system. Since our methods are agnostic to the qubit architecture and the physical implementation is not integral to understanding our results, we do not further discuss details on the specific systems here. For detailed Hamiltonians, Lindblad operators, and a discussion on the pulse end times $T$, see Supplementary material A.

A solution to the Lindblad Eq. (1) for a specific set of pulses $z(t)$ is described by a trace- preserving, completely positive operator called a quantum channel $\mathcal{E}_z$, s.t. $\rho_T = \mathcal{E}_z(\rho_0)$ [29]. For each specific gate $U \in \{R_X(\theta_i), R_Y(\theta_i), R_Z(\theta_i), R_{ZZ}(\theta_i)\}$ to be created, the goal is to optimize the fidelity given by

$$\min_z F(\mathcal{E}_z, \hat{U}) := \min_z \frac{\sum_j \text{Tr}\left(UP_j^\dagger U^\dagger \mathcal{E}_z(P_j)\right) + d^2}{4^N d + d^2}, \tag{2}$$

as in [30]. Here, $N$ is the number of qubits and $d$ is the dimension of the qubit system. For Rydberg systems, $d = 3^N$, and for Cat systems, $d = 2^N$. $P_j$ are the Pauli matrices (for Rydberg extended to a three-dimensional system), of which there are $4^N$. Using the software package Boulder Opal, we optimize the pulses $z(t)$ for the cost function in Eq. (2), using the package's standard convergence criteria [6, 31]. For all problems in this work, we optimize $M = 20$ equidistant predefined angles $\{\theta_i\}_i^M$ in the parameter space $[0, \pi]$.

### 2.2. Pulse clustering

After having optimized the pulses for discrete fixed parameters $\{\theta_i\}_i^M$, these need to be partitioned in corresponding solution branches, or families. Here, we detail our method of clustering pulses in a fixed number of families using *spectral clustering* [21]. This method sorts the nodes $V$ of a weighted graph $G = (V, E, w)$ into a fixed number of clusters. $E$ are the edges of the graph, and $w$ are the weights on these edges encoding the similarity of two nodes. To apply this method to the discrete pulse sorting, we define a fully connected graph, where each node $i$ corresponds to one of the optimized pulses found for a specific parameter $\theta_i$, as shown in **Figure 2**. The weights are set as $w(z_1, z_2) = (\mathrm{dist}(z_1, z_2) + \epsilon)^{-1}$, where dist is some distance on the space of pulses and $\epsilon = 10^{-4}$ is a small regularization parameter. As a basic approach, the $L_2$ distance [32] can be used as

$$L_2(z_1, z_2) = \int_0^T |z_1(t) - z_2(t)|^2 dt. \tag{3}$$

This distance function is often implemented as it is efficient to compute. However, it does not fully serve our needs, since it does not capture shifts on the time axis well. The $L_2$ distance only compares pulse values pointwise in time (see **Figure 3**, where the highest peak shifts, causing a big $L_2$ distance between the pulses even though they are quite similar in shape). As long as two pulses do not overlap, a large time shift causes the same maximal $L_2$ distance as a small shift. To remedy this issue, the Wasserstein-2 distance [33] can be used. This distance has its origins in the mathematical framework of optimal transport and defines the cost of moving one distribution onto another, which is more closely related to our intuitive likeness of pulses (see **Figure 3**). The important point to understand is that the Wasserstein-2 distance treats the pulses as distributions on the plane $\mathbb{R}^2$ and calculates the cost

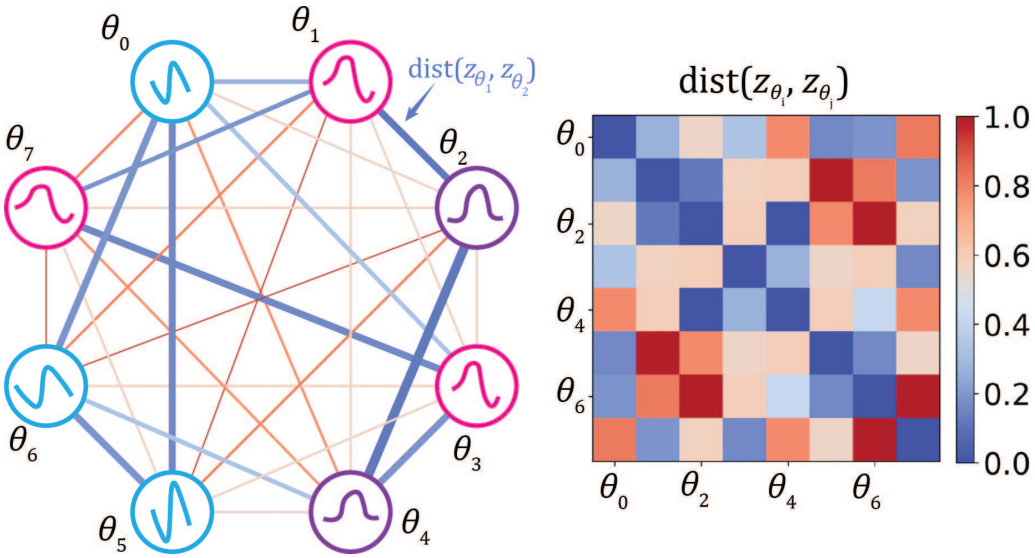


**Figure 2** • To distinguish between different pulse families, pulses are represented as nodes in a graph with the edge weighs between them equal to some distance function $d$. The spectral clustering algorithm takes as input the distance matrix (right), and creates clusters minimizing the distances between pulses of the same cluster.

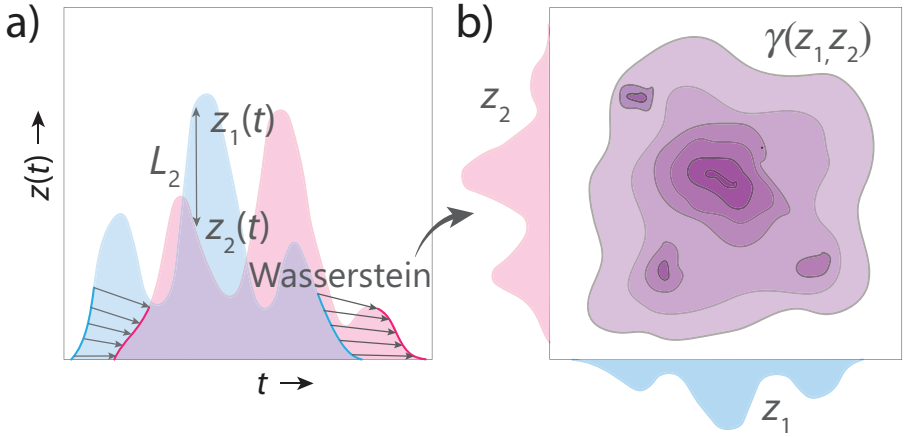


**Figure 3** • Example of Wasserstein-2 vs. $L_2$ distance. (a) If two pulses are compared in $L_2$ distance, both small and large time shifts can result in maximal dissimilarity. The Wasserstein-2 distance is able to capture these shifts because it tries to transport one pulse onto the other. (b) Example of a coupling $\gamma \in \Pi$ between pulses $z_1$ and $z_2$; the Wasserstein-2 distance aims to construct a minimal coupling in the sense of (A.14).

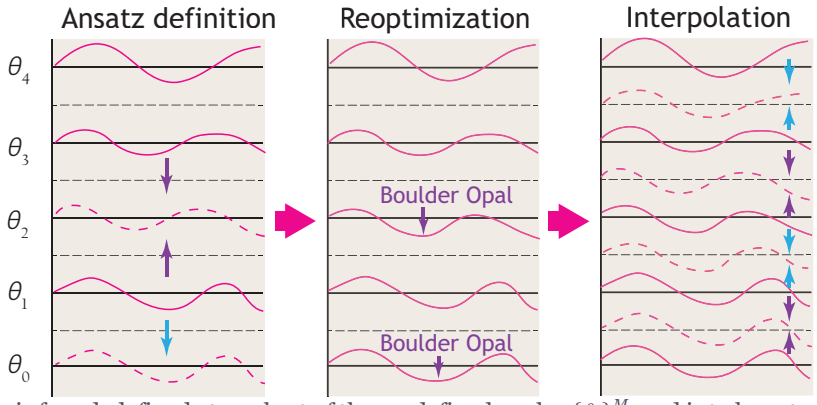


**Figure 4** • A family of pulses is found, defined at a subset of the predefined angles $\{\theta_i\}_i^M$, and is to be extended to all predefined angles. First, ansatzes are created by interpolation if the unassigned angle is within the range of assigned angles, or else set as the highest or lowest found pulse. These ansatzes are optimized using Boulder Opal to extend the family to all predefined angles $\theta_i$. Pulses can then be interpolated within a family in order to find high-fidelity pulses for the entire parameter space.

of moving one onto the other and defines this as the distance [34]. The exact definition of the distance is rather mathematically involved, and therefore deferred to Supplementary material B. [1]

Using one of the previously defined distances, a similarity matrix consisting of the edge weights $w$ can be constructed, see **Figure 2**. This serves as the input for the spectral clustering algorithm. As the spectral clustering algorithm requires a fixed number of clusters, we determine the best possible number of clusters by means of the *Elbow method* [36]. This heuristic determines the point at which an additional cluster does not capture the pulse differences better, and over-fitting starts. For this work this value is always found to be 3 clusters, but in more complex problems with high dimensional parameters, could definitely be expected to increase.

### 2.3. Pulse interpolation

After the originally optimized pulses have been partitioned into families by the clustering algorithm, the following step is to extend the families to the entire parameter space by means of interpolation. In this work, the parameter space will always be $\theta \in [0, \pi]$ so that we can refer to angles. For multiparameter gates, an analogous approach can be pursued.

For each family, we want to first construct pulses on all of $\{\theta_i\}_i^M$, instead of only the subset assigned to it in the clustering. Consider one of the families, there will be a lowest and highest angle assigned to this family in the clustering. Note that a family does not necessarily include only subsequent angles, but might include gaps between disjoint regions. If an angle $\theta_i$ is not assigned to this family and is in such as gap, we take a linear interpolation as an ansatz and optimize the pulses using Boulder Opal. For fixed angles $\theta_i$ outside this range, we simply use the lowest or highest angle pulse as an ansatz and optimize. Employing these ansatzes, hopefully a pulse is found for a parameter that belongs to the same family (reminiscent of the Tikhonov regularization [19]). This leaves us with several extended families of pulses $Z_j$ on all predefined parameters $\{\theta_i\}_i^M$ (see **Figure 4**).

Using linear interpolation within a single family, new pulses can be constructed for all parameters in the parameter space, finalizing our construction of a continuous gate set for each family.

Linear interpolation is computationally very efficient, especially when compared to constructing pulses from the ground up. By interpolating within a family, we expect higher fidelities than if we were to interpolate on the original set of pulses.

## 3. Results

### 3.1. Distance function comparison

This section contrasts the effectiveness of clustering families for the Wasserstein-2 and $L_2$ distances. For arbitrarily optimized pulses, there is no established family structure to validate against. In order to straightforwardly compare the distance measures, we construct $J$ mock families of pulses $Z_j = \{z_{\theta_{j,i}}\}_i^M$. The pulses within one family are constructed in such a way that pulses $z_{\theta_i}$ and $z_{\theta_j}$ look alike for $i$ close to $j$, as they would in actual applications. The exact details of this are left for Supplementary material C. For each angle $\theta_i$, a corresponding pulse $z_{\text{true},i}$ from a family $Z_{\text{true},i} \in \{Z_1, \ldots, Z_J\}$ is randomly picked for the final pulses. This mimics the pulses found by the Boulder Opal optimization procedure and accrues a set of pulses as in **Figure 5b**, of which we have knowledge on the family structure.

On these mock pulses, the distance metrics are compared by constructing a distance matrix as in **Figure 5** and having the spectral clustering algorithm assigned to each pulse $i$ a family $Z_{\text{dist},i} \in \{Z_1, \ldots Z_J\}$. The conditional probability $\mathbb{P}_{\text{dist}}$ of finding a correct match is approximated as

$$\mathbb{P}(\text{cor.}|\text{fnd.}) \approx \frac{\sum_{i,j} \mathbb{1}[Z_{\text{dist},i} = Z_{\text{dist},j}]\mathbb{1}[Z_{\text{true},i} = Z_{\text{true},j}]}{\sum_{i,j} \mathbb{1}[Z_{\text{dist},i} = Z_{\text{dist},j}]}. \quad (4)$$

The reason for choosing this figure of merit is that when two pulses are found to be matching, they only lead to high fidelity as long as they belong to the same family. Missing a match because two pulses from the same family are clustered in different families will not lead to faulty interpolations, and is thus less important from a fidelity perspective (nevertheless, the Wasserstein-2 distance also outperforms the $L_2$ distance in terms of missed matches). **Figure 5** shows the comparison between the two distances. Wasserstein-2 can be seen to largely outperform the standard $L_2$ distance, as it is able to capture the pulse family characteristics

[1] For the Wasserstein-2 distance, pulses are discretized as point clouds with points equidistant along the curve, and the Sinkhorn-Knopp algorithm [35] is used to identify the minimizing coupling.

better due to its transport-based nature. In the rest of this work, the Wasserstein-2 distance is employed for clustering.

### 3.2. Interpolation of gates

To test our clustering method for the interpolation of pulses, we first optimize for $M = 20$ equidistant angles $\theta_i \in [0, \pi]$ for $R_X(\theta), R_Y(\theta), R_Z(\theta)$, and $R_{ZZ}(\theta)$ for both Rydberg and Cat qubits. This allows us to gather results on a universal set of gates on two vastly different systems, showing the versatility and robustness of our method.

The pulses are clustered using our spectral clustering method from Section 2.2, where the Elbow method indicates that for all considered applications, the optimal number of clusters is 3. The families found are extended to the entire $M = 20$ predefined angles $\{\theta_i\}_i^M$ using the methods from Section 2.3. Lastly, for each family, we interpolate the pulses halfway the predefined angles, and determine their fidelity using (2).

**Figure 6** shows the results for the $R_Y(\theta)$ gate on Cat qubits. Generally, the $R_Y$ gate is the most interesting of the three qubit gates because it requires both amplitude and phase control. In **Figure 6a**, we see that when optimizing using Boulder Opal, both the original pulses and the clustered families reach high fidelities, but the interpolation on the original pulses is very bad for almost all angles. For the clustered families, on the other hand, those with good interpolations are found for the entire parameter space. This is highlighted in **Figure 6b**, where the parameter space is partitioned according to where each family performs best, leading to great improvements in the interpolation fidelities compared to the original pulses. **Figure 6c** and **d** further illustrates this by showing that the original pulses are dissimilar for subsequent angles, resulting in low fidelities, whereas the pulses from the families in the highlighted areas correspond well and thus result in high fidelities.

Similar results can be seen in **Figure 7** for the 2-qubit $R_{ZZ}(\theta)$ on a Rydberg system. Here, we see good interpolations of the original pulses around $\theta = \pi/2$, which is also retrieved for one of the families. However, for low and high angles, the interpolation fidelities become quite low for the original pulses (likely due to the presence of many local minima), but high-fidelity pulses are constructed for the clustered families.

**Figure 8** shows all fidelities of interpolated pulses for the problems considered. Across all parameterized gates for both qubit

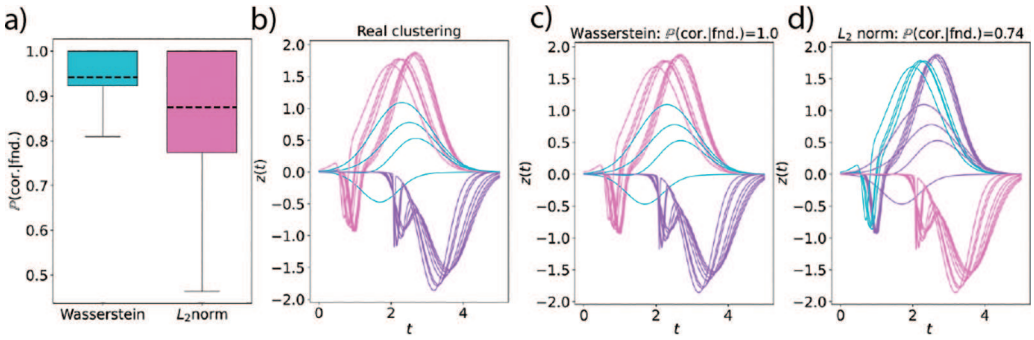


**Figure 5** • Comparison of the Wasserstein-2 and $L_2$ distances for pulse clustering. (a) Box plots of the probability of finding a correct match $\mathbb{P}$(cor.|fnd.) for both distances; data from 2000 trials with $M = 20$ angles in the interval $[0, \pi]$ randomly selected from three pulse families. (b) Example of the authentic clustering of optimized pulse solutions. (c) Clusters found by the Wasserstein-2 distance for the pulses from (b). (d) Clusters found by the $L_2$ distance for the pulses from (b).

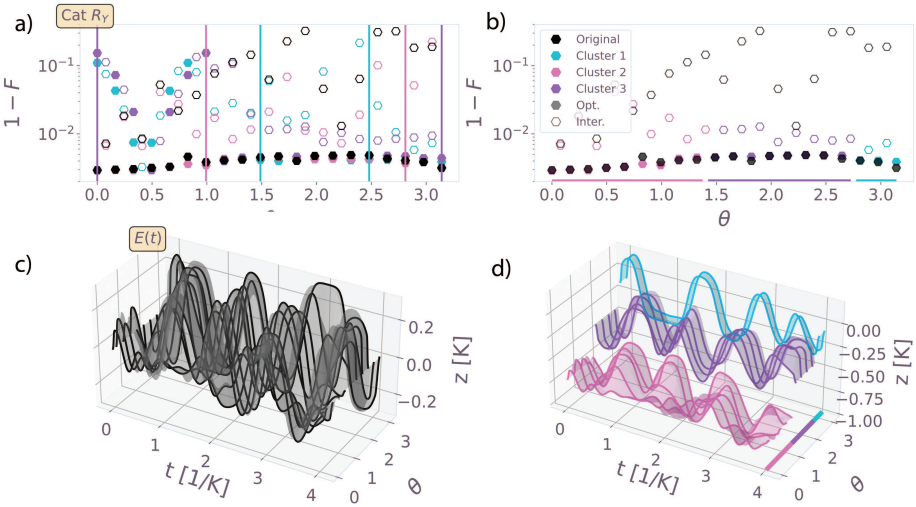


**Figure 6** • Optimization and interpolation results for $R_Y(\theta)$ gate on a Cat qubit system. (a) Black, original pulses and interpolations. Colored pulses show optimized and extended clusters plus interpolations, showing matching or improved interpolation infidelities. Vertical lines are min and max angles of each cluster in the original set of pulses. (b) Narrowed-down results from (a) where the best clusters for each regime of angles are shown, highlighting improvements in fidelity. (c) Single-photon drive $E(t)$ for the original set of pulses, showing a jagged interpolation landscape leading to low fidelities. Horizontal lines indicate chosen regime for each cluster in (d). (d) Clustered pulses for the chosen regimes, showing more regular landscape, necessary for faithful interpolations. Individual clusters are somewhat displaced on the $z$-axis for visibility.

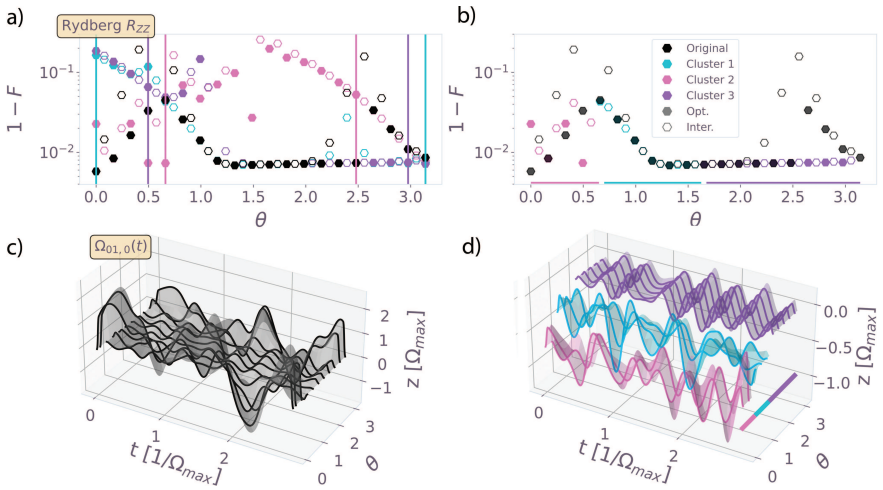


**Figure 7** • Optimization and interpolation results for a $R_{ZZ}(\theta)$ gate on a Rydberg neutral atom qubit system. (a) Black, original pulses and interpolations, for which interpolations have low fidelities for small and large angles. Colored pulses show optimized and extended clusters plus interpolations, showing matching or improved interpolation infidelities. Vertical lines are min and max angles of each cluster in the original set of pulses. (b) Narrowed-down results from (a) where the best clusters for each regime of angles is chosen, highlighting improvements in fidelity. (c) Coupling strength of $|0\rangle \leftrightarrow |1\rangle$ transition on qubit 0 $\Omega_{01,0}(t)$ for the original set of pulses, showing a jagged interpolation landscape leading to low fidelities. Horizontal lines indicate chosen regime for each cluster in (d). (d) Clustered pulses for the chosen regimes, showing more regular landscape, necessary for faithful interpolations. Individual clusters are somewhat displaced on the $z$-axis for visibility.

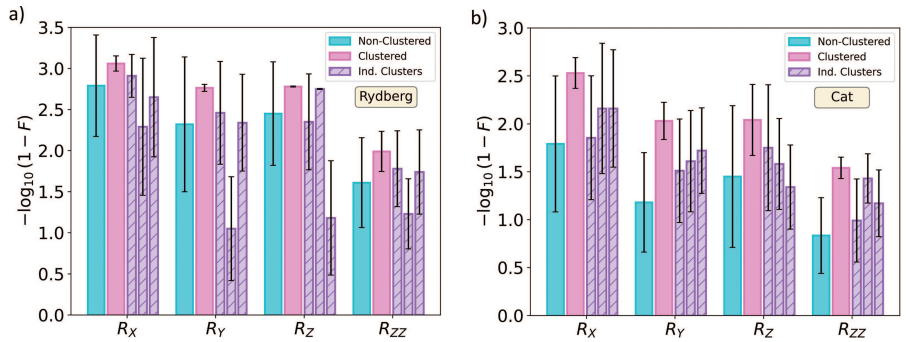


**Figure 8** • Average and standard variations of infidelities of interpolations halfway between optimized angles, as in **Figures 6** and 7. Nonclustered pulses are the original pulses (cyan), three clustered pulses are shown (purple), and the fully clustered method is shown where the parameter space is split up in regimes where the best cluster is assigned (pink). Note the higher mean fidelities as well as much lower standard variations, indicating better interpolations over the entire parameter space. (a) Rydberg gates and (b) Cat qubit gates.

types, there is an increase of half up to a full order of magnitude in fidelity. Partitioning the parameter space with specific families (Clustered, pink results) results in a big advantage in both mean and variance of the fidelities compared to individual clusters (purple). Here individual clusters would be comparable to the Tikhonov regularization method as in [19], since ansatzes for pulse optimization are used. Along the same lines, especially note the much smaller variances of the fidelities indicating that our partition-clustered method yields good pulses over the entire parameter space instead of only in a specific region. The individual family method definitely results in good interpolations for certain regions of parameter space, but multiple families seem to be necessary to patch together a faithful continuous gate set over the entire parameter space. This hails especially true for the Cat qubits, as seen from the fidelities in Fig. 8, which is a more complex optimization problem where likely many local minima in parameter/fidelity space exist.

## 4. Discussion

This work discusses and analyzes a new method for constructing continuous parameter gate sets based on the clustering of pulse families. This is an important problem as for virtually all NISQ-era applications, parameterized gates are required, and optimizing for each individual parameter necessary in a problem is extremely computationally expensive and slow. In our method, spectral clustering using a similarity measure based on Wasserstein-2 distances results in multiple families of pulses on which interfamily interpolation can be performed. The advantage of this method is that multiple families of pulses are found, and among these, the best ones can be selected for a specific regime of the parameter space. This method will prove to be useful for experimental realization, where one family is possibly easier to implement than another. On all gates and on both qubit systems considered, our method leads to significantly better fidelities and much more consistent interpolations than would be the case for original pulse optimization or Tikhonov- based feedforward methods (individual family). In this study, we highlight the great performance of the Cat qubits system, which shows the importance of our method in increasingly more important complex qubit schemes.

In future work, we hope to extend these methods to multiple parameter gates, which might be implemented in more complex VQA- or QAOA-type problems. Furthermore, we are curious to

see the influence of directly optimizing the fidelity via the quantum channel, thus optimizing more directly for the losses, instead of optimizing the unitary evolution and post-processing the influences of the Lindbladian terms. Different parameters have different optimal gate end times, we wish to extend our methods to accommodate for varying gate times instead of one fixed optimal gate time for the largest parameter value ($\theta = \pi$ in this work). Lastly, we hypothesize that a more sophisticated way of interpolation, potentially based on the Wasserstein-2 transport or on the Hamiltonian dynamics, will yield better fidelities for the interpolated pulses.

## Acknowledgments

We thank Klaas Wijnsma, Jasper Postema, Madhav Mohan, Julian Teske, Kisa Barkemeyer, Kara Maller, Luke Visser, and Oliver Tse for fruitful discussions.

## Funding

This research is financially supported by the Dutch Ministry of Economic Affairs and Climate Policy (EZK), as part of the Quantum Delta NL program, by the Horizon Europe program HORIZON-CL4-2021-DIGITAL-EMERGING-01-30 via the project 101070144 (EuRyQa), and by the Netherlands Organisation for Scientific Research (NWO) under Grant No. 680.92.18.05.

## Author contributions

Conceptualization, R.K., J.S. and A.C.; methodology, R.K. and A.C.; software, J.S. and R.K.; validation, A.C. and S.K.; formal analysis, R.K. and J.S.; investigation, J.S. and R.K.; resources, A.C. and S.K.; data curation, J.S., R.K. and A.C.; writing–original draft preparation, R.K.; writing–review and editing, J.S. and A.C.; visualization, R.K. and J.S.; supervision, A.C. and S.K.; project administration, A.C. and S.K.; funding acquisition, A.C. and S.K. All authors have read and agreed to the published version of the manuscript.

## Conflict of interest

The authors declare no conflict of interest.

## Data availability statement

The data and code supporting the findings are available from the corresponding author upon reasonable request.

## Institutional review board statement

Not applicable.

## Informed consent statement

Not applicable.

## Supplementary materials

The supplementary materials are available at https://doi.org/10.20935/AcadQuant7374.

## Additional information

Received: 2024-07-31

Accepted: 2024-09-24

Published: 2024-10-23

*Academia Quantum* papers should be cited as *Academia Quantum 2024*, ISSN 3064-979X, https://doi.org/10.20935/AcadQuant7374. The journal's official abbreviation is *Acad. Quant.*

## Publisher's note



## Copyright



## References

1. Deutsch DE, Barenco A, Ekert A. Universality in quantum computation. Proc R Soc London Series A Math Phys Sci. 1995;449(1937):669–77. doi: 10.1098/rspa.1995.0065
2. de Keijzer RJPT, Colussi VE, Skoric B, Kokkelmans SJJMF. Optimization of the variational quantum eigensolver for quantum chemistry applications. AVS Quantum Sci. 2022;4(1):013803. doi: 10.1116/5.0076435
3. Preskill J. Quantum computing in the NISQ era and beyond. Quantum. 2018;2:79. doi: 10.22331/q-2018-08-06-79
4. Mohan M, de Keijzer R, Kokkelmans S. Robust control and optimal Rydberg states for neutral atom two-qubit gates. Phys Rev Res. 2023;5:033052. doi: 10.1103/PhysRevResearch.5.033052
5. Jandura S, Pupillo G. Time-optimal two- and three-qubit gates for Rydberg atoms. Quantum. 2022;6:712. doi: 10.22331/q-2022-05-13-712
6. Ball H, Biercuk MJ, Carvalho ARR, Chen J, Hush M, Castro LAD, et al. Software tools for quantum control: improving quantum computer performance through noise and error suppression. Quantum Sci Technol. 2021;6(4):044011. doi: 10.1088/2058-9565/abdca6
7. Knill E, Leibfried D, Reichle R, Britton J, Blakestad RB, Jost JD, et al. Randomized benchmarking of quantum gates. Phys Rev A. 2008;77:012307. doi: 10.1103/PhysRevA.77.012307
8. Caneva T, Calarco T, Montangero S. Chopped random-basis quantum optimization. Phys Rev A. 2011;84:022326. doi: 10.1103/PhysRevA.84.022326

9. de Keijzer R, Tse O, Kokkelmans S. Pulse based variational quantum optimal control for hybrid quantum computing. Quantum. 2023;7:908. doi: 10.22331/q-2023-01-26-908

10. Lacroix N, Hellings C, Andersen CK, Di Paolo A, Remm A, Lazar S, et al. Improving the performance of deep quantum optimization algorithms with continuous gate sets. PRX Quantum. 2020;1(2). doi: 10.1103/prxquantum.1.020304

11. Grange C, Poss M, Bourreau E. An introduction to variational quantum algorithms for combinatorial optimization problems. 4OR. 2023;21(3):363–403. doi: 10.1007/s10288-023-00549-1

12. Cerezo M, Arrasmith A, Babbush R, Benjamin SC, Endo S, Fujii K, et al. Variational quantum algorithms. Nat Rev Phys. 2021;3(9):625–44. doi: 10.1038/s42254-021-00348-9

13. Sauvage F, Mintert F. Optimal control of families of quantum gates. Phys Rev Lett. 2022;129:050507. doi: 10.1103/PhysRevLett.129.050507

14. Luchi P, Turro F, Quaglioni S, Wu X, Amitrano V, Wendt K, et al. Control optimization for parametric Hamiltonians by pulse reconstruction. Eur Phys J A. 2023;59(9):196. doi: 10.1140/epja/s10050-023-01108-2

15. Li JS, Ruths J, Yu TY, Arthanari H, Wagner G. Optimal pulse design in quantum control: a unified computational method. Proc Nat Acad Sci. 2011;108(5):1879–84. doi: 10.1073/pnas.1009797108

16. Shi Y, Castelli AR, Wu X, Joseph I, Geyko V, Graziani FR, et al. Simulating non-native cubic interactions on noisy quantum machines. Phys Rev A. 2021;103:062608. doi: 10.1103/PhysRevA.103.062608

17. Preti F, Calarco T, Motzoi F. Continuous quantum gate sets and pulse-class meta-optimization. PRX Quantum. 2022;3:040311. doi: 10.1103/PRXQuantum.3.040311

18. Schilling M, Preti F, Müller MM, Calarco T, Motzoi F. Exponentiation of parametric Hamiltonians via unitary interpolation; 2024. arXiv:2402.01498.

19. Chadwick JD, Chong FT. Efficient control pulses for continuous quantum gate families through coordinated re-optimization. In: 2023 IEEE International Conference on Quantum Computing and Engineering (QCE). Los Alamitos, CA, USA: IEEE Computer Society; 2023. p. 1286–94. doi: 10.1109/QCE57702.2023.00145

20. Rokach L, Maimon O. In: Maimon O, Rokach L, editors. Clustering methods. Boston, MA: Springer US; 2005. p. 321–52. doi: 10.1007/0-387-25465-X15

21. Ng A, Jordan M, Weiss Y. On spectral clustering: analysis and an algorithm. Adv Neural Inf Process Syst. 2001;14:3–4.

22. Saffman M. Quantum computing with atomic qubits and Rydberg interactions: progress and challenges. J Phys B Atom Mol Opt Phys. 2016;49(20):202001. doi: 10.1088/0953-4075/49/20/202001

23. Morgado M, Whitlock S. Quantum simulation and computing with Rydberg-interacting qubits. AVS Quantum Sci. 2021;3(2):023501. doi: 10.1116/5.0036562

24. Vikstal P, Garcia-alvarez L, Puri S, Ferrini G. Quantum approximate optimization algorithm with cat qubits; 2023. arXiv:2305.05556.

25. Grimm A, Frattini NE, Puri S, Mundhada SO, Touzard S, Mirrahimi M, et al. Stabilization and operation of a Kerr-cat qubit. Nature. 2020;584(7820):205–9. doi: 10.1038/s41586-020-2587-z

26. Matekole ES, Fang YLL, Lin M. Methods and results for quantum optimal pulse control on superconducting qubit systems. In: Quantum 2.0 Conference and Exhibition. Optica Publishing Group; 2022. p. QM3A.2. doi: 10.1364/QUANTUM.2022.QM3A.2

27. Carvalho ARR, Ball H, Biercuk MJ, Hush MR, Thomsen F. Error-robust quantum logic optimization using a cloud quantum computer interface. Phys Rev Appl. 2021;15:064054. doi: 10.1103/PhysRevApplied.15.064054

28. Brasil CA, Fanchini FF, Napolitano RdJ. A simple derivation of the Lindblad equation. Rev Bras Ensino Fís. 2013;35:1–9. doi: 10.1590/S1806-11172013000100003

29. Caruso F, Giovannetti V, Lupo C, Mancini S. Quantum channels and memory effects. Rev Mod Phys. 2014;86:1203–59. doi: 10.1103/RevModPhys.86.1203

30. Nielsen MA. A simple formula for the average gate fidelity of a quantum dynamical operation. Phys Lett A. 2002;303(4):249–52. doi: 10.1016/S0375-9601(02)01272-0

31. Q-CTRL. Boulder opal; 2023 [cited 2024 Aug 2]. Available from: https://q-ctrl.com/boulder-opal

32. Yosida K. Functional analysis. Vol. 123. Heidelberg: Springer Science & Business Media; 2012.

33. Santambrogio F. Optimal transport for applied mathematicians. Heidelberg: Birkäuser; 2015.

34. Villani C. Topics in optimal transportation. Vol. 58. Providence (RI): American Mathematical Society; 2021.

35. Knight PA. The Sinkhorn–Knopp algorithm: convergence and applications. SIAM J Matrix Anal Appl. 2008;30(1): 261–75. doi: 10.1137/060659624

36. Yuan C, Yang H. Research on K-value selection method of K-means clustering algorithm. J. 2019;2:226–35. doi: 10.3390/j2020016